Cancer Chemotherapy and Pharmacology (2019) 83:237–254
https://doi.org/10.1007/s00280-018-3726-1

ORIGINAL ARTICLE

6-MOMIPP, a novel brain-penetrant anti-mitotic indolyl-chalcone, inhibits glioblastoma growth and viability

Shengnan Du[1] · Jeffrey G. Sarver[2] · Christopher J. Trabbic[2] · Paul W. Erhardt[2] · Allen Schroering[1] · William A. Maltese[1]

Received: 5 June 2018 / Accepted: 3 November 2018 / Published online: 13 November 2018

Abstract

Purpose 3-(6-Methoxy-2-methyl-1H-indol-3-yl)-1-(4-pyridinyl)-2-propene-1-one (6-MOMIPP) is a novel indole-based chalcone that disrupts microtubules. The present study aims to define the mechanism through which 6-MOMIPP induces cell death and to evaluate the efficacy of the compound in penetrating the blood–brain barrier and inhibiting growth of glioblastoma xenografts.

Methods The effects of 6-MOMIPP were evaluated in cultured U251 glioblastoma cells, using viability, flow cytometry, and tubulin polymerization assays. Scintillation proximity and tubulin crosslinking methods were used to identify the binding site of 6-MOMIPP on tubulin, and western blots were performed to define the signaling pathways that contribute to cell death. LC/MS assays were used to study the pharmacokinetic behavior of 6-MOMIPP in mice. Subcutaneous and intracerebral xenograft models were utilized to assess the effects of 6-MOMIPP on growth of U251 glioblastoma in vivo.

Results The findings indicate that 6-MOMIPP targets the colchicine site on β-tubulin. At concentrations ≥ 250 nm, 6-MOMIPP induces mitotic arrest, caspase activation and loss of cell viability. Cells are protected by caspase inhibitors, pointing to an apoptotic mechanism of cell death. Loss of cell viability is preceded by activation of Cdk1(Cdc2) and phosphorylation of Bcl-2 and Bcl-xL. Inhibition of both events with a Cdk1 inhibitor prevents cell death. 6-MOMIPP has broad activity against the viability of multiple glioblastoma, melanoma and lung carcinoma cell lines. Viability of normal cells, including differentiated neurons, is not significantly affected at a drug concentration (1 μM) that reduces viability in most cancer lines. Pharmacokinetic studies in mice show that concentrations of 6-MOMIPP in the brain mirror those in the plasma, indicating that 6-MOMIPP readily penetrates the blood–brain barrier. Studies with mice bearing human U251 glioblastoma xenografts demonstrate that 6-MOMIPP is effective in suppressing growth of subcutaneous and intracerebral tumors without causing general toxicity.

Conclusions The results indicate that 6-MOMIPP is a novel microtubule disruptor that targets the colchicine binding site on β-tubulin to induce mitotic arrest and cell death. The ability of 6-MOMIPP to penetrate the blood–brain barrier and inhibit growth of glioblastoma xenografts suggests that it warrants further preclinical evaluation as potential small-molecule therapeutic that may have advantages in treating primary and metastatic brain tumors.

Keywords Microtubules · Glioblastoma · Anti-mitotic · Chalcone · Cell death · Apoptosis

Introduction

Microtubule-targeting agents (MTAs) are widely used as anti-cancer drugs [1, 2]. They can be classified into two major groups: (1) Microtubule-stabilizing agents, such as paclitaxel, which inhibit microtubule depolymerization; and (2) Microtubule-disrupting agents, such as *Vinca* alkaloids and colchicine, which interfere with microtubule assembly [2, 3]. Although they bind to different sites on β-tubulin [4], these MTAs have a similar basis for their potent anti-cancer

Electronic supplementary material The online version of this article (https://doi.org/10.1007/s00280-018-3726-1) contains supplementary material, which is available to authorized users.

✉ William A. Maltese
william.maltese@utoledo.edu

[1] Department of Cancer Biology, University of Toledo College of Medicine and Life Sciences, 3000 Transverse Drive, Toledo, OH 43614, USA

[2] Center for Drug Design and Development, University of Toledo College of Pharmacy and Pharmaceutical Sciences, 2810 W. Bancroft Street, Toledo, OH 43606, USA

effects. By perturbing highly dynamic mitotic spindle assemblies, MTAs arrest mitotic progression and eventually kill cancer cells through mitotic catastrophe or apoptosis [5–8]. Despite their widespread use, MTAs are not without drawbacks, including acquired resistance [2] and dose-limiting myelosuppression and neurotoxicity [1].

Among the challenges in cancer treatment, perhaps none is greater than the need for more effective therapies for brain tumors, including primary lesions like glioblastoma [9, 10] and secondary tumors that originate from metastatic spread of cancers from other tissues [11]. Established MTAs like the *Vinca* alkaloids and taxanes have limited utility in these settings because of their relatively poor passage across the blood–brain barrier [12–15]. Thus, ongoing studies continue to seek new MTAs with properties that may overcome the current limitations.

Commencing with the early work of Edwards et al. [16], studies have shown that synthetic chalcones resembling the naturally occurring flavonoid precursor, 1,3-diphenyl-2-propen-1-one, have anti-proliferative activities when applied to cancer cells in vitro [17–20]. Chalcone analogs in which one phenyl ring of the prototypical structure is replaced with a modified indole, while the other phenyl ring is substituted with a trimethoxyphenyl, have proven to be particularly effective antineoplastic agents in vitro [21, 22] and in subcutaneous tumor xenografts in mice [23, 24].

Our laboratory has been working with synthetic chalcones broadly characterized as indolyl-pyridinyl-propenones (IPPs). We previously reported that some compounds of this class, most notably *trans* 3-(5-methoxy-2-methyl-1H-indol-3-yl)-1-(4-pyridinyl)-2-propene-1-one (abbreviated MOMIPP), can induce a unique form of non-apoptotic cell death termed 'methuosis' in glioblastoma and a wide variety of other cancer cells [25, 26]. While performing structure–activity relationship studies to define the features of IPPs that are required for induction of methuosis, we discovered that seemingly subtle modifications of the indole ring resulted in major alterations of biological activity, yielding compounds with the ability to disrupt microtubule architecture [27]. In particular, moving the methoxy group on MOMIPP from the 5′ position to the 6′ position on the indole ring (yielding 6-MOMIPP) was sufficient to switch the biological activity of the compound from methuosis to microtubule-disruption [28].

In the present study we extend our investigation of 6-MOMIPP to establish its mechanism of action and evaluate its anti-tumor efficacy *in vitro* and in glioblastoma xenograft models. The results indicate that 6-MOMIPP interacts with the colchicine binding site on β-tubulin to induce mitotic arrest and cell death by a caspase-dependent mechanism. Most importantly, 6-MOMIPP readily crosses the blood–brain barrier (BBB) and exhibits significant activity against both subcutaneous and intracerebral glioblastoma. Therefore, 6-MOMIPP and related IPPs merit further preclinical evaluation as potential therapeutic agents for treatment of primary and metastatic brain tumors.

Methods

Chemicals

6-MOMIPP, was synthesized as described previously [28]. The compound was serially diluted in dimethylsulfoxide (DMSO) to achieve the desired final concentration in tissue culture medium with 0.1% DMSO. BMS-265246 (Selleckchem), SP600125 (Cayman Chemical), z-LEHD-fmk (R&D Systems, Inc.) and pro-VAD-fmk (Vergent Bioscience) were purchased from the indicated sources and dissolved in DMSO. *N,N′*-Ethylenebis iodoacetamide (EBI) was from Toronto Research Chemicals. XenoLight D-Luciferin—K^+ salt bioluminescent substrate was purchased from Perkin Elmer. NMP and Solutol-HS15 were from Sigma-Aldrich.

Cell culture

U251 human glioblastoma cells were obtained from the Development Therapeutics Program (DTP) Tumor Repository, NCI Division of Cancer Treatment and Diagnosis (DCTD). Cells were maintained in Dulbecco's modified Eagle medium (DMEM), supplemented with 10% (v/v) fetal bovine serum (FBS) (JR Scientific), at 37 °C with 5% CO_2/95% air. Cultures were periodically tested for *Mycoplasma* contamination by staining with 4′,6-diamidino-2-phenyl-indole (DAPI) or use of the PlasmoTest assay (InVivogen) and were confirmed to be negative. Information about the origin and culture conditions for other cell lines tested for susceptibility to 6-MOMIPP can be found in Online Resource 1.

Cell viability

Viability of cells in vitro was assessed by measuring cellular ATP using the CellTiter-Glo® luminescence assay according to the manufacturer's protocol (Promega Corp). U251 cells were seeded in white-walled opaque 96-well plates (6250 cells/cm^2), with four replicate wells for each culture condition. After addition of compounds at the indicated concentrations, cell viability was assayed at a 48 h end-point. Luminescence was quantified with a Berthold Tech Centro XS3 LB 960 luminometer, using the preinstalled MikroWin software. To compensate for differences in growth rate, other cell lines were seeded at densities noted in Online Resource 1.

Phase contrast and immunofluorescence imaging

For live cell imaging studies, cells were seeded in 35 mm dishes at 12,500 cells/cm^2 and incubated for 24 h before commencing treatment with compounds. Cells were examined by phase contrast microscopy using an Olympus IX70 inverted microscope equipped with a heated stage, a DP80 digital camera, and CellSens™ software (Olympus America). Immunofluorescence visualization of microtubule architecture was carried out as described previously [27]. Briefly, cells were plated on glass coverslips in 60 mm dishes at 16,700 cells/cm^2 and compounds were added 1 day after plating. Cells were fixed with cold methanol and incubated for 1 h with a monoclonal antibody against α-tubulin (Cat. No. T5168, Sigma Chemical Co.) at 1:100 dilution, followed by Alexa Fluor 568-labeled goat anti-mouse IgG (ThermoFisher Scientific) (1:600, 1 h). Nuclear DNA was stained with DAPI for 5 min.

Cell cycle analysis

Cells were seeded in 60 mm dishes at 16,700 cells/cm^2. On the next day, the sub-confluent cells were treated with 6-MOMIPP or other compounds at the concentrations indicted in the figure legends. After 24 h the cells were harvested by trypsinization, fixed in ice-cold 70% ethanol, washed twice by centrifugation/resuspension in phosphate-buffered normal saline (PBS), and then suspended in 900 µl PBS containing 6.25 mM $MgSO_4$ and 1 mM $CaCl_2$. After incubation at room temperature for 15 min, 2 µl of a 100 mg/mL solution of RNase A was added and cells were incubated at 37 °C for 15 min. Finally, 100 µl of a 500 mg/ml aqueous solution of propidium iodide was added and the cells were analyzed with a Becton–Dickinson FACS-Calibur flow cytometer. DNA histograms were generated with CellQuest Pro software.

Tubulin polymerization in intact cells

The polymerization state of microtubules in intact cells was analyzed by flow cytometry essentially as described by Morrison et al. [29]. Cells were plated in 60 mm dishes at 14,300 cells/cm^2. After 1 day, while cells were still sub-confluent, cells were treated with the indicated concentrations of 6-MOMIPP, colchicine, paclitaxel or an equivalent volume of DMSO for 24 h. Cells were harvested and pelleted by centrifugation (600×*g*, 5 min), then fixed for 10 min in 1 ml microtubule-stabilizing buffer (80 mM PIPES, pH 6.8, 1 mM $MgCl_2$, 5 mM EDTA, 0.5% Triton X-100) containing 0.5% glutaraldehyde. The glutaraldehyde was quenched by adding 0.7 ml PBS containing 1 mg/ml $NaBH_4$ and the cells were collected by centrifugation (1000×*g*, 5 min). The cell pellet was re-suspended in 100 µl of antibody-diluting solution (PBS, pH 7.4, 0.2% Triton X-100, 2% bovine serum albumin, and 0.1% NaN3) containing 50 µg/ml RNase (Qiagen) for an overnight incubation at 4 °C. Samples were then incubated in the dark for 3 h with 25 µl of anti-α-tubulin–FITC conjugate (Sigma, 1:50 dilution). Tubulin fluorescence of individual cells was analyzed with a Becton–Dickinson FACS-Calibur flow cytometer.

Immunoblot analysis

Cells were seeded in 10 cm dishes at 22,700 cells/cm^2 in DMEM containing 10% FBS. After 24 h, while cells were still sub-confluent, fresh medium containing the indicated compounds or an equivalent volume of DMSO was added and cells were harvested after 24 or 48 h. Cells were lysed in sodium dodecyl sulfate (SDS) sample buffer [30] and the protein concentration was determined by colorimetric assay using Bio-Rad reagent (Bio-Rad, Inc.). Equal amounts of protein (80 µg) were subjected to SDS–polyacrylamide gel electrophoresis (SDS–PAGE), transferred to polyvinylidene difluoride membrane, and analyzed by immunoblot procedures described previously [31]. Chemiluminescent signals were quantified using an Alpha Innotech FluorChem HD2 imaging system with Alpha View software. Mouse monoclonal antibody against β-tubulin (Cat. No. sc-5274,) was purchased from Santa Cruz Biotechnology. All of the following antibodies were obtained from Cell Signaling Technology: Rabbit anti-caspase-9 (Cat. No. 9502S); rabbit anti-cleaved caspase-3 (Asp175) (Cat. No. 9661S); rabbit anti-caspase-7 (Cat. No. 9492S); rabbit anti-pospho-SAPK/JNK (Thr183/Tyr185) (Cat. No. 9251S); rabbit anti-SAPK/JNK antibody (Cat. No. 9252s); rabbit anti-Bcl-xL (54H6) (Cat. No. 2764s); rabbit anti-phospho-Bcl-2 (Ser70) (5H2) (Cat. No. 2827s); rabbit anti-phospho-c-Jun (Ser63) (Cat. No. 9261S); rabbit anti-c-Jun (60A8) (Cat. No. 9165s); rabbit anti-PP1α (Cat. No. 2582S); and rabbit anti-phospho-PP1α (Thr320) (Cat. No. 2581S). Rabbit anti-phospho-BcL-xL (Ser62) (Cat. No. PA535496) was obtained from Thermo Fisher Scientific. Mouse monoclonal anti-phospho-histone H3 (Ser10) (Cat. No. 05-806) was purchased from Sigma. Horseradish peroxidase (HRP)-coupled goat anti-mouse IgG (Cat. No. 554002) and goat anti-rabbit IgG (Cat. No. 554021) were from BD Biosciences.

Scintillation proximity assay

For the colchicine competition assay, [^{3}H]colchicine (ring C, methoxy-^{3}H, 1 mCi/ml, SA = 60–87 Ci/mmol) was purchased from PerkinElmer and diluted 1/20 into ethanol. 10 µl of the diluted [^{3}H]colchicine (0.5 µCi) was added to each well in a 96-well white-walled plate (PerkinElmer) and air-dried for 1 h. Then 90 µl of ice-cold binding buffer (80 mM PIPES, pH 6.8, 1 mM $MgCl_2$, 1 mM EGTA, 1 mM GTP) was added,

followed by escalating concentrations of 6-MOMIPP, colchicine or vinblastine in 1 µl water. For this purpose, 6-MOMIPP was first dissolved in a solvent composed of 7.5% NMP, 15% Solutol-HS15, and 77.5% PBS to concentration of 1.3 mM, and serial dilutions were prepared in deionized water. Biotin-labeled β-tubulin and GTP were purchased from Cytoskeleton, Inc. The biotinylated tubulin (0.5 µg) was added to the assay in 10 µl ice-cold binding buffer and the reaction mixture was incubated at 37 °C for 2 h. Finally, 0.08 mg streptavidin-yttrium silicate (YSI) beads (PerkinElmer) were added in 20 µl binding buffer, and incubation was continued for 15 min. The signal emitted from the interaction between [^{3}H]-colchicine on biotinylated tubulin and streptavidin-YSI beads was quantified with a Packard TopCount®NXT™ Microplate Scintillation & Luminescence Counter. Results were plotted using GraphPad Prism 7.

[^{3}H]Vinblastine was obtained from PerkinElmer (0.25 mCi/ml, SA = 20.8 Ci/mmol). For the vinblastine competition assay, 0.5 µCi of [^{3}H]vinblastine was diluted into 10 µl ethanol, and added to the wells of a white-walled 96-well plate to air dry for 1 h. Then unlabeled vinblastine, colchicine, or 6-MOMIPP (final concentrations 0.24 µM or 2.4 µM) were added along with 1 µg biotinylated tubulin in 80 µl cold binding buffer. Reaction mixtures were incubated at 37 °C for 2 h, with 4 replicates for each condition. Streptavidin-YSI beads (0.4 mg suspended in 50 µl binding buffer) were added to each reaction mixture and scintillation signals were quantified after 15 min as described above.

Tubulin crosslinking and drug binding assay

The ability of 6-MOMIPP to protect key residues in the colchicine binding site of β-tubulin from crosslinking by EBI was adapted from a published procedure [32]. U251 cells were seeded in 10 cm dishes at 22,700 cells/cm^2 and allowed to attach for 24 h. Thereafter, the sub-confluent cells were pretreated for 4 h with 6-MOMIPP, paclitaxel, colchicine or an equivalent volume of DMSO at concentrations indicated in Fig. 3c. EBI was then added to the medium at a final concentration of 100 µM, and incubation was continued for 1.5 h. Cells were harvested and lysed in SDS sample buffer, and protein concentration was determined by the Bio-Rad colorimetric assay. For each sample 80 µg protein was subjected to SDS–PAGE and transferred to PVDF membrane. Immunoblot assays were performed as described earlier, using a mouse monoclonal antibody against β-tubulin (Santa Cruz Biotechnology, Cat. No. sc-5274).

Pharmacokinetics and tissue distribution of 6-MOMIPP in vivo

Swiss Webster mice (8–10 weeks, female) were purchased from Charles River Laboratories and housed in ventilated cages on a 12 h light–dark cycle. 6-MOMIPP was dissolved in NSP (7.5% *N*-methyl-2-pyrrolidone, 15% Solutol-HS15, 77.5% PBS) to generate a 2 mg/ml solution and administered to mice via intraperitoneal (ip) injection at a dose of 20 mg/kg. Mice were euthanized at intervals of 30 min, 1 h, 2 h, 4 h, and 8 h after drug administration. Blood was collected by cardiac puncture, stored on ice in EDTA-coated collection tubes, and centrifuged at 10,000×*g* for 20 min to obtain plasma. Thereafter, plasma was stored at − 80 °C until analysis. Brain and liver were snap-frozen in liquid nitrogen and stored at − 80 °C until analysis. Frozen tissues were weighed and homogenized 1:9 (w/v) in RIPA buffer (150 mM NaCl, 1% NP40, 0.5% sodium deoxycholate, 1% SDS, 50 mM Tris, pH 7.5).

To determine the concentration of 6-MOMIPP, plasma (200 µl) or tissue homogenate (500 µl) were extracted with 1 ml ethyl acetate by incubating at 37 °C for 20 min, followed by centrifugation for 2 min at 16,000×*g*. An 800 µl aliquot of supernatant was vacuum centrifuged at 30 °C for 1 h and the residue was suspended in 100 µl of 30% (v/v) acetonitrile, 0.1% (v/v) formic acid in deionized water. Liquid chromatography separations were performed on a Waters 2795 HT-Alliance LC Separations Module with a 10 µl sample injection onto a Waters Ascentis Express C18 column (75 × 21 mm, 2.7 µm) with matching guard column. Isocratic elution was performed with 30% (v/v) organic phase composed of acetonitrile, and 70% aqueous phase made up of deionized water containing 0.1% (v/v) formic acid, at a total flow rate of 0.3 ml/min. 6-MOMIPP was detected via multiple reaction monitoring (MRM) on a Micromass Quattro Micro Mass Spectrometer in ESI + mode with capillary voltage 3.0 kV, source temperature 100 °C, desolvation temperature 400 °C, desolvation gas flow 650 l/h, cone gas flow 40 l/h, and dwell time 0.2 s. 6-MOMIPP was detected as 293.1 > 95.9 at cone voltage 40V, collision energy 23V, and at a column retention time of 2.1 min. Plasma sample measurements were calibrated using standards prepared in commercial EDTA-treated mouse plasma purchased from Pel-Freez Biologicals (Rogers, AZ, USA). Brain and liver homogenate samples were calibrated using RIPA homogenates made from brain and liver tissues, respectively, collected from untreated control mice. Standards were spiked to give a known concentration of MOMIPP in units of nM; i.e., nmol/l for plasma, or nmol/kg for brain and liver homogenates, with the latter based on the tissue mass contained in the homogenates (9 µl RIPA buffer added per mg tissue). Plasma levels of 6-MOMIPP were measured based on plasma volume and expressed as nM concentration. Brain and liver homogenate levels were measured based on tissue mass prior to homogenization, so that these concentrations represent nmol/kg tissue. For ease of comparison, tissue densities were approximated as 1.0 g/ml, so that brain and liver levels could be expressed as nM concentration.

Anti-tumor efficacy studies in xenograft models

Athymic CrTac:NCR-Foxn1<nu>mice (female, 7–8 weeks) were purchased from Taconic Biosciences (Rensselaer, NY). For generation of glioblastoma xenografts suitable for bioluminescence imaging (BLI), U251 human glioblastoma cells were transfected with a vector (pCMV5-Neo-pGL3) encoding firefly luciferase, and a stable cell line was generated by clonal selection in medium containing G418. The resulting cell line, termed U251-LUC, was maintained in DMEM supplemented with 10% (v/v) FBS and 200 µg/ml G418 and was periodically tested for uniform luciferase expression in vitro.

To initiate subcutaneous (sc) xenografts, mice received flank injections of 5×10^6 U251-LUC cells suspended in 100 µl DMEM with 50% Matrigel (Corning Life Science). After 4 days, when a small mass was palpable, each mouse was subjected to BLI in an IVIS Spectrum imaging system (PerkinElmer), 15 min after receiving an ip injection containing 0.3 mg D-luciferin in PBS. Mice with tumors detectable by BLI were allocated randomly into control or treatment groups. Thereafter, the mice in the treatment group received 20 mg/kg 6-MOMIPP via ip injection every 12 h for 14 days, while controls received injections of vehicle (NSP). Mice were weighed periodically throughout the study and tumor growth was monitored by BLI at the indicated intervals. Upon termination of the study, final luminescence images were acquired and all tumors were excised and weighed. The study was repeated twice, once with 8 mice per group, and once with 11–12 mice per group.

The orthotopic glioblastoma xenograft model was established in athymic mice based on a previously published method [33]. Each mouse received an intracerebral injection of 4×10^5 U251-LUC cells. Tumor growth was monitored by BLI. By the fourth day, all of the mice had tumors that emitted 10^7–10^8 photons when injected with D-luciferin as described earlier. Mice bearing tumors were grouped randomly into control and treatment groups and 6-MOMIPP (20 mg/kg) or vehicle was administered by ip injection every 12 h for 12 consecutive days. Mice were weighed and monitored for signs of toxicity or neurological impairment throughout the treatment period. Upon termination of the study, a final bioluminescence scan was performed and the brains were fixed in 10% neutral buffered formalin. At the same time, blood was collected by cardiac puncture, stored in lithium heparin-coated collection tubes (ThermoFisher), and centrifuged at 10,000×*g* for 20 min to isolate plasma. The plasma samples were utilized for toxicity screens with a comprehensive diagnostic profile kit and a VetScan VS2 Analyzer (Abaxis), following standard protocols recommended by the manufacturer.

Histology

Fixed brains bearing intracerebral tumors were embedded in paraffin and serial coronal sections were prepared, moving anterior-to-posterior in 100 µm steps. At each step three 5 µm sections were mounted and stained with hematoxylin and eosin (H&E). Central regions of the tumors were identified and images were obtained with an Olympus Virtual Slide Microscope VS120. CellSense™ software was used to draw contours around the tumors and determine the tumor area. For each brain, the mean tumor area was determined from four separate sections in the central part of the tumor.

Statistical analysis

GraphPad Prism 7 was used for statistical analysis. For studies in vitro, statistical significance of differences between control and treated cells in culture groups was determined using Student's unpaired *t* test. For comparisons of BLI, tumor weight, or tumor areas in control vs. treated groups of mice at specific times, the Mann–Whitney test for unpaired samples was used. Values of $p \leq 0.05$ were considered to be significant.

Results

6-MOMIPP induces mitotic arrest and caspase-dependent death in glioblastoma cells

The structure of 6-MOMIPP is depicted in Fig. 1a. When U251 glioblastoma cells were treated with 1 µM 6-MOMIPP, the majority of cells rounded up and detached from the culture dish within 24 h, and the few remaining attached cells contained multiple micronuclei (Fig. 1a). Flow cytometry analysis revealed that cells treated with 6-MOMIPP at concentrations ranging from 0.25 to 5.0 µM for 24 h were arrested in the G2/M phase of the cell cycle (Fig. 1b). Upon continued incubation with anti-mitotic concentrations of 6-MOMIPP for 48 h, DNA histograms of the combined floating and attached cells demonstrated accumulation of a sub-G1/G0 population, suggestive of cell death (Fig. 1c). Very similar effects were observed when 6-MOMIPP was tested in a different human glioblastoma cell line, T98G (Online Resource 1). Viability assays based on measurement of cellular ATP confirmed loss of cell viability by 48 h (Fig. 1d). These observations are consistent with the propensity of prolonged mitotic arrest to trigger cell death via apoptosis [7, 34] or mitotic catastrophe, wherein faulty segregation of chromosomes leads to nuclear abnormalities and eventual death by caspase-dependent or caspase-independent mechanisms [5, 35].

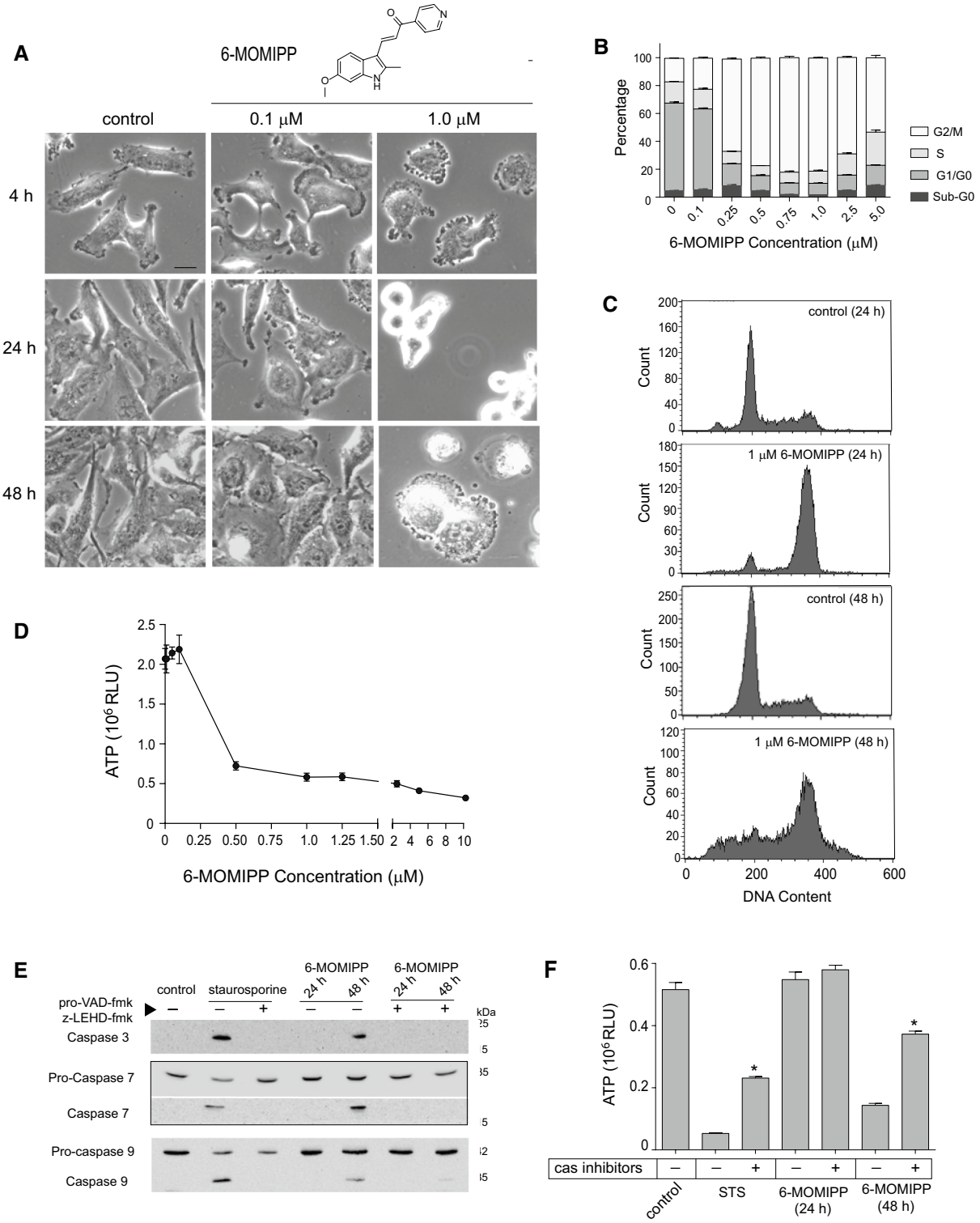

To ascertain if cell death induced by 6-MOMIPP was accompanied by activation of caspases, we assessed the status of initiator (caspase 9) and executioner (caspases 3 and 7) caspases at 24 h and 48 h after addition of the compound, using staurosporine as a positive control for induction of apoptosis (Fig. 1e). Cleaved (active) forms of all three caspases were not observed at 24 h, but were readily detected at 48 h after addition of 6-MOMIPP, coinciding with the accumulation of sub-G0 cells and the decline in cellular ATP. To determine if cell death was caspase-dependent, cells

◂**Fig. 1** Effects of 6-MOMIPP on morphology, cell cycling and viability of U251 glioblastoma cells. **a** U251 cells were seeded in 35 mm dishes and treated with DMSO or the indicated concentrations of 6-MOMIPP. Phase contrast images were acquired at the indicated time points. The bar in the 4 h control panel represents 20 µm. **b** Cells were treated for 24 h with increasing concentrations of 6-MOMIPP and flow cytometry was performed after staining the cells with propidium iodide. The percentage of cells in each phase of the cell cycle was determined from DNA histograms using CellQuest software ($n=3$ at each drug concentration). **c** Examples of DNA histograms are shown for cells exposed to 1 µM 6-MOMIPP for 24 h or 48 h, revealing accumulation of sub-G1/G0 cells at the later time point. **d** Cells were treated with 6-MOMIPP at the indicated concentrations for 48 h and ATP was measured by CellTiter-Glo® luminescence assay as described in the "Methods". Values represent the mean ± SD of four replicates. **e** Cells were treated with 1 µM 6-MOMIPP or the equivalent volume of DMSO for 24 h or 48 h. Separate cultures were co-treated with 6-MOMIPP and caspase inhibitors (Pro-VAD-fmk and z-LEHD-fmk), which were added 2 h before the 6-MOMIPP. Cells treated with staurosporine served as positive controls for caspase activation. Cells (attached and detached) were harvested and lysed in SDS sample buffer and subjected to immunoblot analysis for the indicated caspases, as described in the "Methods". The results are representative of three separate experiments. **f** U251 cells were treated with DMSO (control), staurosporine (positive control for apoptosis) or 1 µM 6-MOMIPP, with or without caspase inhibitors. Cell viability was assessed at 24 h or 48 h using the CellTitre Glo® ATP assay. Values are the mean (± SD) of four replicates. *Increases in viability observed with addition of caspase inhibitors were significant at $p<0.05$

were treated with 6-MOMIPP in the presence or absence of a broad-spectrum caspase inhibitor, pro-VAD-fmk, plus a caspase-9 inhibitor, z-LEHD-fmk. (The latter was included because in our hands pro-VAD-fmk does not completely inhibit activation of caspase 9). The results depicted in Fig. 1e, f indicated that the inhibitor cocktail blocked caspase activation in the cells treated with staurosporine or 6-MOMIPP and provided significant protection from cell death.

Effects of 6-MOMIPP on viability extend to other tumor cell lines

We next broadened the evaluation of 6-MOMIPP to include several additional glioblastoma cell lines, as well as cell lines representative of cancers that frequently give rise to brain metastases (melanoma and lung cancer). The results shown in Online Resource 2 indicate that all of the tested cell lines responded to 6-MOMIPP with a decline in cell viability (ATP) by 48 h. However, there were some marked differences in sensitivity to 6-MOMIPP. For example, within the glioma group, U87MG and A172 cells were much less sensitive than U251 or T98G (Online Resource 2A). Similarly, within the melanoma group, the SK-MEL-2 line was less sensitive than any of the others tested (Online Resource 2C). In clinical settings, acquired drug resistance in recurrent tumors often results in failure of chemotherapy. Thus, in this study we also included two drug-resistant cell lines: U251-TMZR, glioblastoma cells selected for temozolomide resistance [36], and H125-CPR, a lung carcinoma line selected for cisplatin-resistance. Both cell lines exhibited significant responses to 6-MOMIPP, although viability was not decreased as much as in the corresponding parental cell lines (Online Resource 2A &B).

Finally, we examined the effects of 6-MOMIPP in non-transformed cells (Online Resource 2D). Viability of normal human skin fibroblasts or HUVEC was not significantly decreased after 48 h with 1 µM 6-MOMIPP, a concentration that was effective in most of the cancer cell lines. At 5 µM, the effects of 6-MOMIPP on the viability of fibroblasts and HUVEC were comparable to the weaker responses obtained in some of the tumor cell lines (e.g., U87MG, A172). To assess the possibility of neuronal toxicity, we tested the effects of 6-MOMIPP on RN46A-B14 cells, a SV40 large T antigen-immortalized rat neuron progenitor cell line that can be induced to differentiate into non-dividing cells with neuronal morphology [37]. Viability of the differentiated neuronal cells was not reduced with either 1 µM or 5 µM 6-MOMIPP, and cell morphology was not noticeably altered after 48 h (Online Resource 2E).

6-MOMIPP causes microtubule depolymerization by targeting the colchicine binding site on β-tubulin

Morphological rounding and mitotic arrest are features typically observed in cells treated with drugs that target microtubules. In a previous study, we found that indolyl pyridinyl propenones related to 6-MOMMIP caused cell rounding, surface blebbing and tubulin depolymerization within 4 h [27]. Likewise, we found that cell rounding and blebbing are early effects of 6-MOMIPP [28]. These features are consistent with the effects of direct microtubule depolymerizing agents. Thus, in the present studies, we extended the examination of 6-MOMIPP to compare it longer-term effects with those of other microtubule-targeting compounds. As shown in Fig. 2a, U251 cells treated with vehicle alone or a sub-lethal concentration of 6-MOMIPP (0.1 µM) exhibited a flattened morphology with a distinct microtubule network. In contrast, the few cells that remain attached to the dish after treatment with 6-MOMIPP at higher concentrations that cause cell cycle arrest and cell death exhibited a diffuse tubulin staining pattern and sometimes contained multiple micronuclei. To further evaluate the tubulin polymerization state, we carried out a flow cytometric analysis that measures polymerized tubulin in intact cells [29]. In this assay, U251 cells were exposed to different concentrations of 6-MOMIPP or a reference microtubule stabilizer (paclitaxel) or destabilizer (colchicine) for 24 h. After washing out soluble tubulin monomers, the polymerized microtubule network was fixed with glutaraldehyde and immunostained with

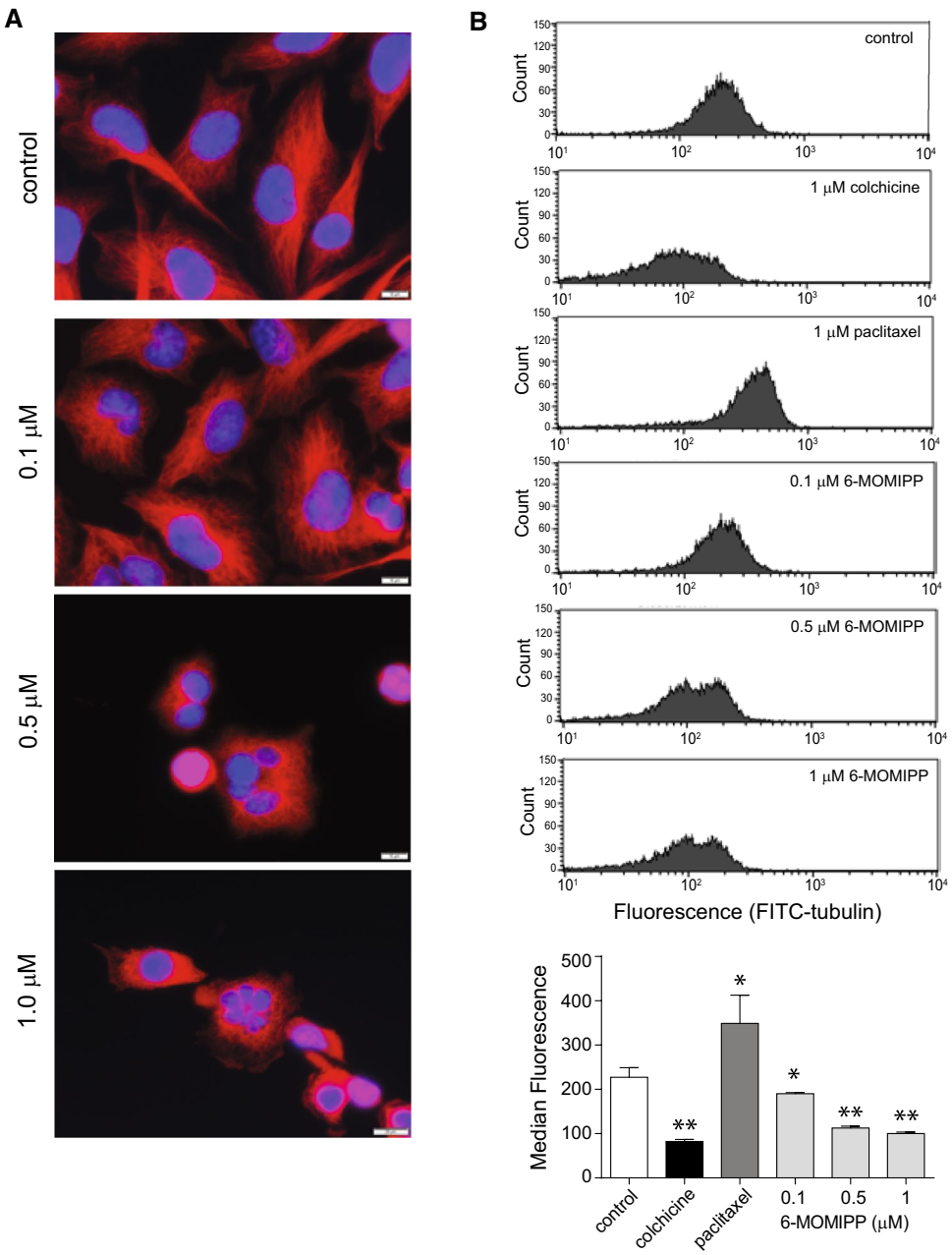

Fig. 2 6-MOMIPP disrupts tubulin polymerization and promotes micronucleation in cultured U251 cells. **a** Cells were treated with DMSO (control) or 6-MOMIPP at the indicated concentrations for 24 h. Microtubules were stained by immunofluorescence, using anti-α-tubulin primary antibody and Alexa Fluor 568-labeled goat anti-mouse secondary antibody (red fluorescence). Nuclei were stained with DAPI (blue fluorescence). **b** To quantify polymerized tubulin, cells were treated with DMSO, colchicine (1 μM), paclitaxel (1 μM) or indicated concentrations of 6-MOMIPP for 24 h. Tubulin monomers were washed out of the cells and polymerized microtubules were fixed, immunostained and analyzed by flow cytometry as described in the "Methods". Representative fluorescence intensity histograms are shown above the bar graph, which depicts the median fluorescence intensity (± SD) determined from three separate cultures. Asterisks denote values that were significantly increased or decreased relative to the controls (*$p < 0.05$; **$p < 0.001$)

FITC-conjugated antibody against α-tubulin. As expected, colchicine significantly reduced the median fluorescence signal of the cell population compared to the DMSO control, indicating tubulin depolymerization (Fig. 2b). The microtubule stabilizer, paclitaxel, did the opposite, substantially increasing the median fluorescence. In cells treated with 6-MOMIPP, the median fluorescence of polymerized tubulin decreased in a concentration dependent manner (Fig. 2b), suggesting that 6-MOMIPP acts in a manner similar to the microtubule destabilizer, colchicine.

Among the various MTAs, colchicine and related compounds bind to a site on β-tubulin that is distinct from the sites targeted by *Vinca* alkaloids and taxanes [38]. To obtain information about how 6-MOMIPP interacts with tubulin, a competition-binding scintillation proximity assay (SPA) was performed [39]. In this assay compounds that can bind to the colchicine site on β-tubulin will compete with [^{3}H] colchicine which, in turn, diminishes the scintillation signal generated when biotinylated β-tubulin containing [^{3}H] colchicine interacts with streptavidin-coated yttrium sensor beads. The results depicted in Fig. 3a demonstrate that 6-MOMIPP was able to substantially inhibit the binding of [^{3}H]colchicine to β-tubulin when added in a concentration range of 1–10 μM. As expected, unlabeled colchicine also diminished the binding of [^{3}H]colchicine, but vinblastine had no effect. In a limited converse study, 6-MOMIPP did

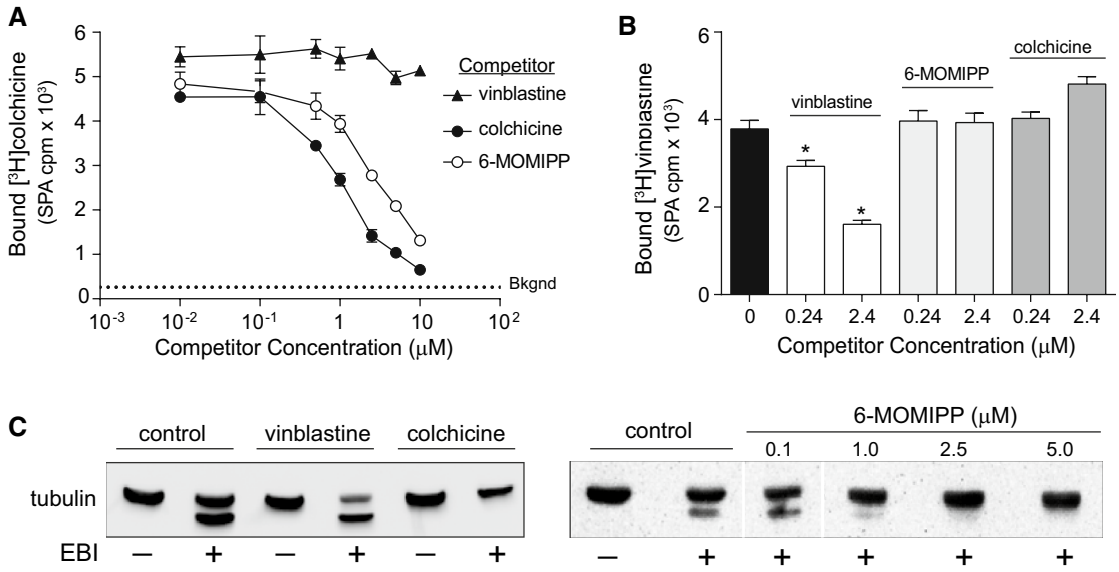

Fig. 3 6-MOMIPP interacts with the colchicine binding site on β-tubulin. **a** [^{3}H]colchicine was incubated with biotin-labeled β-tubulin for 2 h in the presence of unlabeled vinblastine, colchicine or 6-MOMIPP at concentrations of 0.01, 0.10, 0.50, 1.0, 2.5, 5.0 or 10 μM. Streptavidin SPA beads were then added and scintillation signals were quantified as described in the "Methods". Each point represents the mean ± SD of 4 replicates. **b** [^{3}H]vinblastine was incubated for 2 h with biotin-labeled β-tubulin in the presence of unlabeled vinblastine, colchicine or 6-MOMIPP (final concentrations 0.24 μM or 2.4 μM). Streptavidin SPA beads were then added and scintillation signals were quantified. Each point represents the mean ± SD of four replicates. Significant decreases in binding ($p \leq 0.05$) are denoted by asterisks. **c** Cells were pre-incubated for 4 h with DMSO (control), 1 μM vinblastine, 1 μM colchicine, or the indicated concentrations of 6-MOMIPP. The cross-linker, EBI, was then added for 1.5 h and the cells were harvested for SDS–PAGE and immunoblot analysis of tubulin. The results shown are representative of three separate experiments

not compete against binding of [^{3}H]vinblastine to tubulin (Fig. 3b). In that case, only unlabeled vinblastine inhibited the binding of [^{3}H]vinblastine to tubulin. These findings support the notion that 6-MOMIPP associates with β-tubulin at or near the well-defined colchicine binding site.

To obtain additional confirmation of the site of 6-MOMIPP interaction on β-tubulin, we used an alternative approach that is based on the principle that EBI forms a crosslink between two cysteine residues (cys239 and cys354) in the colchicine binding pocket of β-tubulin in living cells. The crosslinking of these cysteine residues generates a mobility shift that can be detected as a faster-migrating band when β-tubulin is subjected to SDS gel electrophoresis [32]. When colchicine occupies its binding site on β-tubulin, EBI access to the target cysteines is blocked. Thus, in this study U251 cells were treated with DMSO, 6-MOMIPP, colchicine, or vinblastine for 4 h followed by 1.5 h incubation with EBI. The cells were then harvested and subjected to SDS–PAGE and immunoblot analysis for β-tubulin. As expected, incubation of cells with colchicine, but not vinblastine, prevented the formation of the faster-migrating EBI-crosslinked band (Fig. 3c). Similar to colchicine, 6-MOMIPP inhibited the formation of the EBI-crosslinked band at concentrations that caused mitotic arrest and microtubule depolymerization (1 μM and above).

Effects of 6-MOMIPP are associated with activation of Cdk1 and phosphorylation of anti-apoptotic Bcl-2 proteins

Activation of Cdk1(Cdc2) promotes key events in the transition from G2 into the mitotic phase of the cell cycle, including disassembly of the nuclear envelope and chromosome condensation [40]. Cdk1 is activated by its binding to Cyclin B1 and dephosphorylation by Cdc25. Upon assembly of mitotic spindles and correct alignment of chromosomes in metaphase, the activity of Cdk1 is switched off by degradation of Cyclin B1 and phosphorylation by Wee1and Myt1 kinases, facilitating mitotic exit [41, 42]. When spindle dynamics and mitotic progression are disrupted by MTAs, Cyclin B1 degradation is inhibited, thereby maintaining Cdk1 in an active state [43].

Anti-apoptotic members of the Bcl-2 family (e.g., Bcl-2 and Bcl-xL) are among the targets of Cdk1 [44], and there is evidence that these proteins are functionally inactivated by phosphorylation [45–47]. Therefore, we explored the possibility that increased phosphorylation of Bcl-2 proteins by Cdk1 could provide a plausible link between 6-MOMIPP-induced microtubule-disruption/mitotic arrest and the initiation of apoptosis. We began by asking whether the activity of Cdk1 was in fact elevated in cells treated with

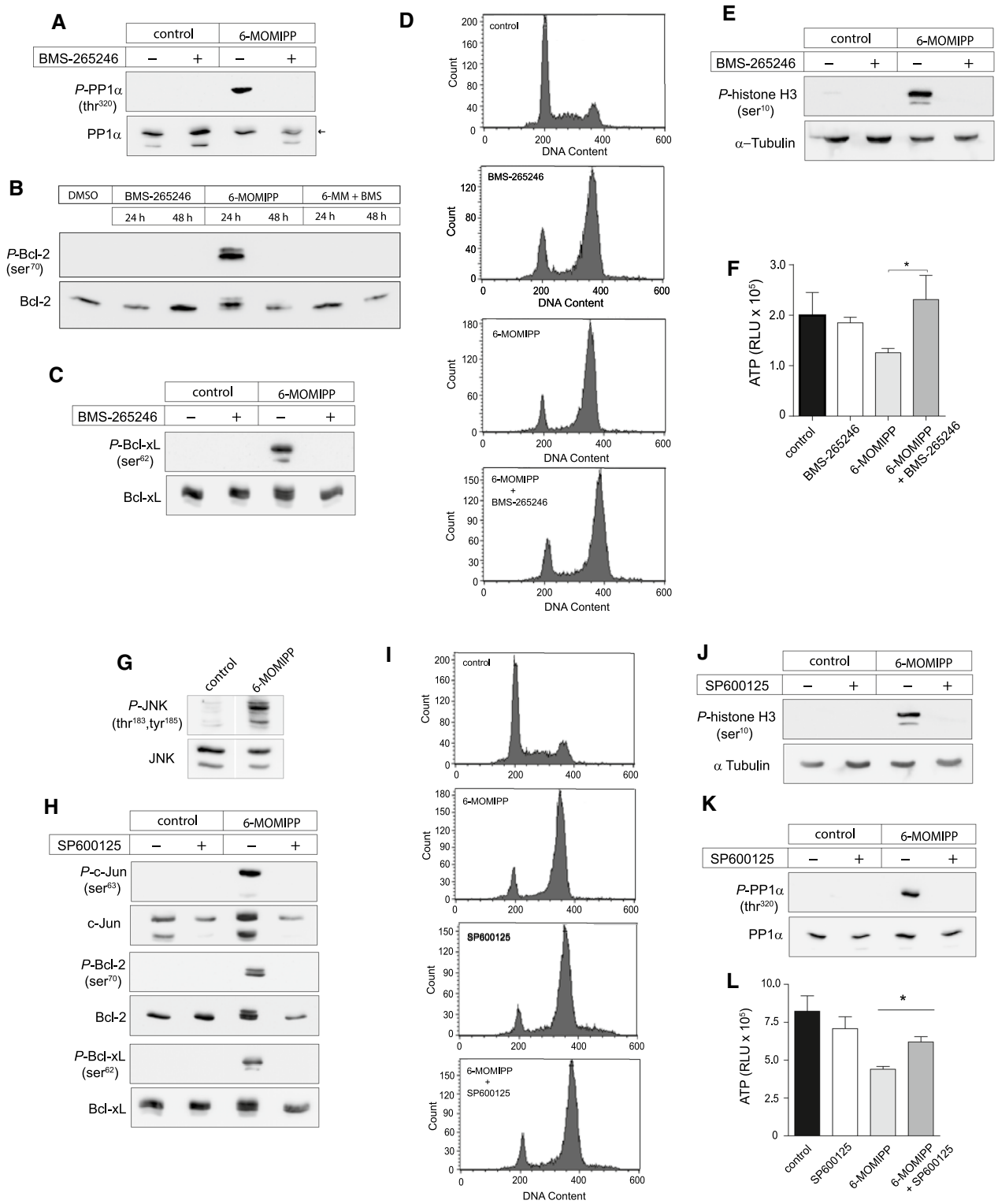

6-MOMIPP. The phosphatase, PP1α, is a known substrate of the Cdk1/Cyclin B1 complex in mitosis, with phosphorylation occurring at thr320 [48]. As shown in Fig. 4a, treatment of U251 cells with 1 μM 6-MOMIPP for 24 h caused readily detectable phosphorylation of thr320 on PP1α, which was completely abolished when BMS-265246, a specific inhibitor of Cdk1 [49], was added together with 6-MOMIPP. The activation of Cdk1 in cells treated with 6-MOMIPP coincided with a marked increase in phosphorylation of Bcl-2 (Fig. 4b). Phosphorylation was maximal at 24 h and then

◂**Fig. 4** Induction of cell death by 6-MOMIPP depends on activation of Cdk1 and phosphorylation of Bcl-2 and Bcl-xL. **a** U251 cells were treated with 1 μM 6-MOMIPP or an equivalent volume of DMSO (control), in the presence or absence of a Cdk1 inhibitor, BMS-265246 (5 μM). After 24 h the detached and attached cells were harvested and equal amounts of protein from the same samples were subjected to SDS–PAGE and immunoblot analysis for phosphorylated vs. total PP1α. **b** Cells were treated with 1 μM 6-MOMIPP or an equivalent volume of DMSO (control) for 24 h or 48 h. Where indicated (MM + BMS), the Cdk1 inhibitor, BMS-265246, was added together with 6-MOMIPP. Immunoblots show the phosphorylated and total Bcl-2 detected in equal aliquots of protein from each sample. **c** Cells were treated with 1 μM 6-MOMIPP or an equivalent volume of DMSO (control) for 24 h. Where indicated, the Cdk1 inhibitor was added together with 6-MOMIPP. Immunoblots show the phosphorylated and total Bcl-xL detected in equal aliquots of protein from each sample. Results similar to those depicted in **a**–**c** were observed in three separate studies. **d** Cells were treated for 24 h with 6-MOMIPP, BMS-265246 or a combination of both (as above) and then stained with propidium iodide and subjected to flow cytometry to acquire DNA histograms. **e** Cells were treated with 1 μM 6-MOMIPP or an equivalent volume of DMSO (control), in the presence or absence of 5 μM BMS-265246, and harvested after 24 h. Equal amounts of protein were subjected to immunoblot analysis for phosphorylated histone H3, with α-tubulin as a loading control. **f** U251 cells were seeded in 96-well plates and CellTiter-Glo® viability assays were performed as described in the "Methods", after 48 h treatment with 1 μM 6-MOMIPP, 5 μM BMS-265246 or a combination of both. The controls were treated with vehicle (DMSO). Values are the mean ± SD of four replicates (* $p < 0.005$). **g** U251 cells were treated with 1 μM 6-MOMIPP or an equivalent volume of DMSO (control) for 24 h, and immunoblot analysis was performed on equal aliquots of protein to detect phosphorylated and total forms of JNK. **h** Cells were incubated for 24 h with 1 μM 6-MOMIPP or DMSO (control). Where indicated, a JNK inhibitor, SP600125 (75 μM), was added 2 h before addition of 6-MOMIPP and maintained throughout the subsequent 24 h incubation. Attached and detached cells were harvested and equal amounts of protein were subjected to immunoblot analysis for the proteins indicated at the left of each blot. Similar results were obtained in three experiments. **i** Cells were treated for 24 h with 1 μM 6-MOMIPP, 75 μM SP600125 or a combination of both, and then stained with propidium iodide and subjected to flow cytometry to acquire DNA histograms. Controls were treated with a volume of DMSO equivalent to that used for the addition of test compounds. **j, k** Cells were treated with 1 μM 6-MOMIPP or an equivalent volume of DMSO (control), in the presence or absence of SP600125 (75 μM). After 24 h, the detached and attached cells were harvested and equal amounts of protein were subjected to SDS-PAGE and immunoblot analysis for **j** phosphorylated and total histone-H3 or **k** phosphorylated and total PP1α. **l** U251 cells were seeded in 96-well plates and CellTiter-Glo® viability assays were performed as described in the "Methods", after 48 h treatment with 1 μM 6-MOMIPP, 5 μM SP600125, or a combination of both. The controls were treated with vehicle (DMSO). Values are the mean ± SD of four replicates (*$p < 0.005$)

diminished at 48 h. The basis for loss of Bcl-2 phosphorylation at 48 h was not investigated further, because it corresponds with loss of ATP and cell viability (Fig. 1c, d), which could affect multiple kinases. Like Bcl-2, the phosphorylation of the anti-apoptotic Bcl-xL was also markedly increased after 24 h treatment with 6-MOMIPP. Most notably, the phosphorylation of both Bcl-2 and Bcl-xL was prevented by inclusion of the Cdk1 inhibitor, BMS-265246, together with 6-MOMIPP (Fig. 4b, c). The Cdk1 inhibitor by itself is predicted to prevent transition of cells from G2 into the M phase of the cell cycle. As depicted in Fig. 4d, the DNA histograms of cells treated with BMS-265246, 6-MOMIPP, or a combination of both, were indistinguishable. However, by assessing the phosphorylation of histone-H3 on ser10, we were able to separate the cell cycle effects of BMS-265246 from those of 6-MOMIPP. Histone-H3 phosphorylation occurs in conjunction with chromatin condensation during mitotic prophase and is maintained through metaphase [50]. Consistent with disruption of spindle microtubules and mitotic arrest, cells treated with 6-MOMIPP alone exhibited robust histone-H3 phosphorylation (Fig. 4e). In contrast, cells treated with BMS-265246, either alone or with 6-MOMIPP, showed no evidence of histone-H3 phosphorylation (Fig. 4e). Therefore, despite the similar DNA histograms (Fig. 4d), cells treated with BMS-265246, with or without 6-MOMIPP, appear to be arrested at an earlier point in either G2 or mitotic prophase, before histone phosphorylation occurs.

Finally, we asked whether preventing 6-MOMIPP-treated cells from becoming arrested in mitosis (with attendant Cdk1 activation and Bcl-2/Bcl-xL phosphorylation) might mitigate the loss of cell viability. BMS-265246 by itself did not affect cell viability (Fig. 4f), but induced a flattened cell morphology (Online Resource 3). When combined with 6-MOMIPP, the Cdk1 inhibitor offered significant protection from loss of viability (Fig. 4f) and prevented the cells from rounding up and detaching from the substratum (Online Resource 3).

6-MOMIPP triggers activation of c-Jun N-terminal kinase

Colchicine and other drugs that cause microtubule depolymerization are known to promote sustained activation of the stress-activated kinase, JNK [51, 52]. JNK activation, as measured by its phosphorylation, has in turn been associated with apoptosis induced by MTAs. Thus, we asked whether treatment of U251 cells with 6-MOMIPP was associated with activation of JNK. The results indicate that both the p54 and p46 splice variants of JNK were robustly phosphorylated in cells exposed to 1 μM 6-MOMIPP for 24 h (Fig. 4g). Consistent with JNK activation, phosphorylation of the established JNK substrate, c-Jun, was increased in cells treated with 6-MOMIPP (Fig. 4h). Induction of JNK activation by MTAs coincides with phosphorylation of anti-apoptotic Bcl-2 and Bcl-xL proteins [53–55]. In accord with these studies, we found that the phosphorylation of Bcl-2 and Bcl-xL triggered by 6-MOMIPP could be blocked by a JNK inhibitor, SP600125 (Fig. 4h). The prevention of Bcl-2/Bcl-xL phosphorylation by the JNK inhibitor appears may

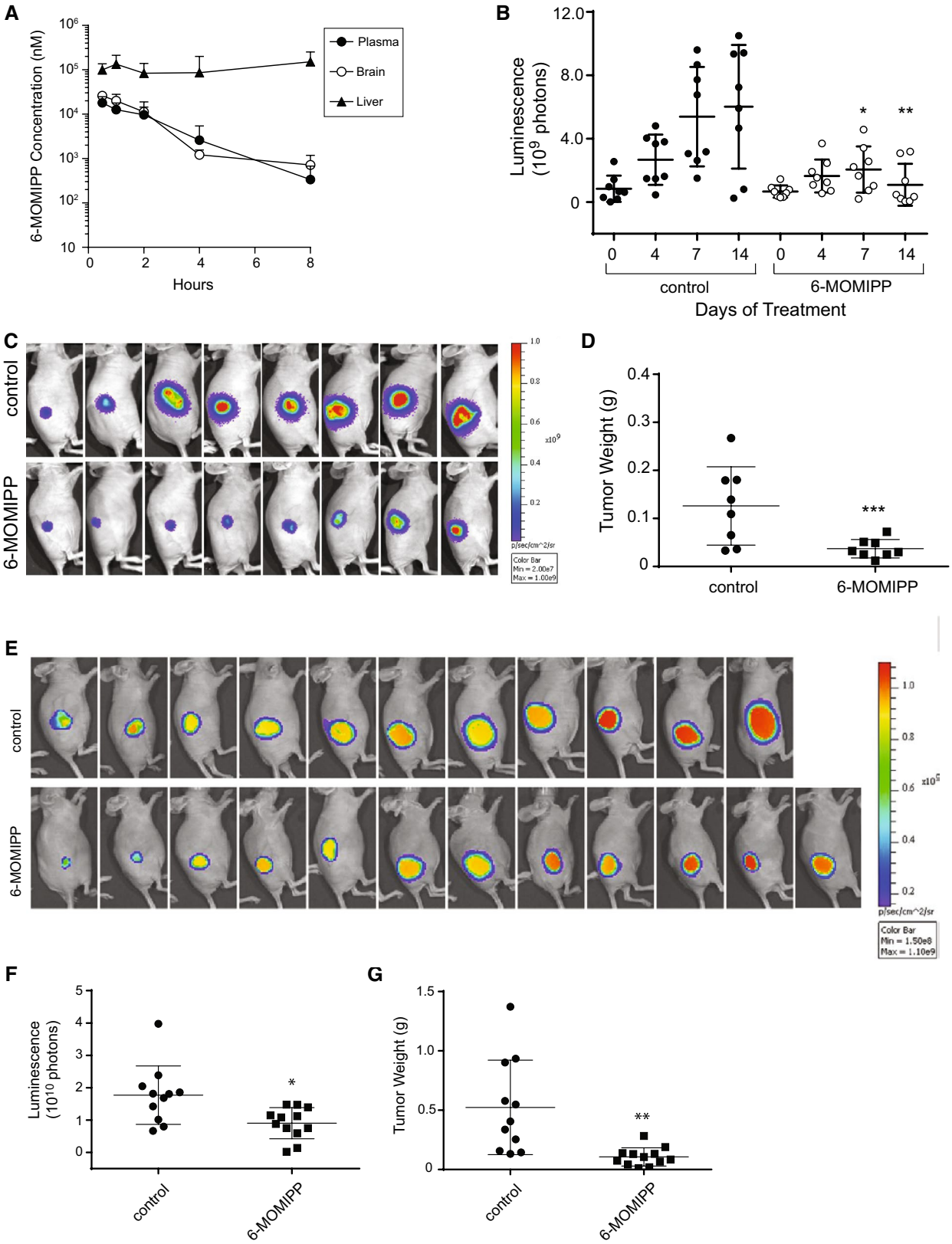
A
6-MOMIPP Concentration (nM)
Plasma
Brain
Liver
Hours
B
Luminescence (10^9 photons)
Days of Treatment
control
6-MOMIPP
C
control
6-MOMIPP
D
Tumor Weight (g)
control
6-MOMIPP
E
control
6-MOMIPP
F
Luminescence (10^10 photons)
control
6-MOMIPP
G
Tumor Weight (g)
control
6-MOMIPP

◂**Fig. 5** Pharmacokinetic properties and efficacy of 6-MOMIPP in subcutaneous glioblastoma xenograft model. **a** Mice received a single ip injection of 6-MOMIPP (20 mg/kg) formulated in NSP. At each time point, mice were euthanized and blood was obtained by cardiac puncture. The liver and brain were immediately frozen in liquid N_2. Tissue samples were homogenized, after which plasma and tissue homogenates were extracted and analyzed by LC-MS/MS assay to determine the concentrations of 6-MOMIPP as described in the "Methods". Each value represents the mean ± SD derived from 6 mice. **b** Immunocompromised mice received sc implants of human U251-LUC cells, as described in the "Methods". When tumors were detectable by BLI at 4 days after implantation, treatment with 6-MOMIPP commenced (20 mg/kg, every 12 h). The start of treatment is designated as day-0. Control mice received an equivalent volume of NSP vehicle. Bioluminescence imaging was performed on all mice in the control and 6-MOMIPP groups ($n=8$ for each group) on the days indicated in the graph (**b**). BLI values in the 6-MOMIPP-treated group were significantly reduced on day-7 ($p<0.01^{*)}$ and day-14 ($p<0.005$**). The bioluminescence images captured on day-14 of the study are shown in **c**. All mice were euthanized on day-14 and tumor wet weight was recorded (**d**). ***The difference in tumor weight between the 6-MOMIPP-treated and control groups was significant at $p<0.005$. **e, f** The previous study was replicated with the following minor modifications: Tumors were initiated with 10^7 cells instead of 5×10^6 cells. Eleven mice were included in the control group and 12 in the treatment group, instead of eight. Mice were treated for 15 days instead of 14 days. **e** Bioluminescence images of individual mice were acquired on the 15th day of treatment. **f** The luminescence signals (photons) from the control and treated mice show a significant decrease on day-15. **g** Tumor wet weights are also significantly decreased after 15-day treatment (mean ± SD). Significance was determined by the Mann-Whitney unpaired test. *$p<0.005$; **$p<0.001$

be related to inhibition of the transition between G2 and mitotic prometaphase. Thus, while treatment of cells with SP600125 alone, or in combination with 6-MOMIPP, produced DNA histograms indicative of G2/M arrest (Fig. 4i), there was no phosphorylation of histone-H3 (a prometaphase marker) (Fig. 4j) or activation of Cdk1 (phosphorylation of PP1α) (Fig. 4k), as there was with 6-MOMIPP alone. As in the case of the Cdk1 inhibitor (Fig. 4f), the addition of a JNK inhibitor together with 6-MOMIPP provided significant protection from the loss of cell viability (Fig. 4l). This supports the notion entry into a state of prolonged mitotic arrest is a key factor in the cell death program induced by 6-MOMIPP.

Pharmacokinetic study of 6-MOMIPP

To assess the pharmacokinetic properties of 6-MOMIPP and evaluate its ability to penetrate the blood–brain barrier (BBB), 6-MOMIPP was initially formulated in several different solvents and administered to mice via oral or intraperitoneal (ip) routes at various dosages. Based on the results of these preliminary studies, we selected NSP (7.5% *n*-methyl-2-pyrrolidone, 15% Solutol HS15, 77.5% phosphate-buffered normal saline) as the optimal vehicle for ip administration of 6-MOMIPP. As shown in Fig. 5a, when mice were given a single injection of the compound at a dose of 20 mg/kg, the plasma concentration exceeded 10 μM after 30 min. The plasma concentration declined with a half-life of approximately 1.3 h, but at 8 h remained above the 0.25 μM threshold shown to cause mitotic arrest in cultured U251 cells (Fig. 1b). Consistent with the behavior of many drugs, liver concentrations of 6-MOMIPP were substantially higher than the plasma levels at all time points. Of particular note, the concentration of 6-MOMIPP in the brain closely mirrored the concentration in the plasma, approaching a brain to plasma ratio near 1.0 throughout the time-course.

Anti-tumor efficacy of 6-MOMIPP in xenograft models

Based on the foregoing studies, we elected to initiate a study to evaluate the effects of 6-MOMIPP on the growth of sc glioblastoma xenografts derived from U251-LUC cells. Beginning four days after implantation of tumors cells, mice received ip injections of 20 mg/kg 6-MOMIPP (or vehicle for controls) twice daily, for a total of 14 days. The BLI results depicted in Fig. 5b, c show that the sc xenografts in the control mice grew aggressively, and that treatment with 6-MOMIPP significantly decreased tumor progression as measured by this method. The end-point tumor weights confirmed that 6-MOMIPP significantly inhibited growth of the sc xenografts (Fig. 5d). The sc xenograft study was carried out a second time with essentially the same results (Fig. 5e–g). 6-MOMIPP was well tolerated, with no behavioral signs of toxicity or loss of body weight during the course of treatment (Online Resource 4A&B).

Considering the efficacy of 6-MOMIPP in suppressing the growth of sc tumors, and the ability of the compound to penetrate the BBB, we extended these studies to an orthotopic glioblastoma xenograft model. The U251 human glioblastoma cell line has been widely used to rapidly establish aggressive intracerebral tumors with many of the pathological features of human glioblastoma [56]. Beginning 4 days after tumor cell implantation, mice bearing intracerebral U251-LUC xenografts were treated with 6-MOMIPP, using the same formulation and dosing regimen applied in the sc xenograft study. The study was terminated after 12 days of treatment (16 days total), when some of the control mice began exhibiting signs of distress. The results of BLI indicated a significant inhibitory effect of 6-MOMIPP on the progression of the intracerebral xenografts (Fig. 6a, b). This was confirmed by end-point morphometric analysis of tumor areas in stained coronal sections through four separate planes of each tumor, which revealed a significant decrease in the size of the tumors in the group of mice treated with 6-MOMIPP (Fig. 6c, d). During the course of the study, there was no significant difference in body weight between the control and treated groups (Online Resource 4C). The blood chemistry profiles of samples collected at the end of

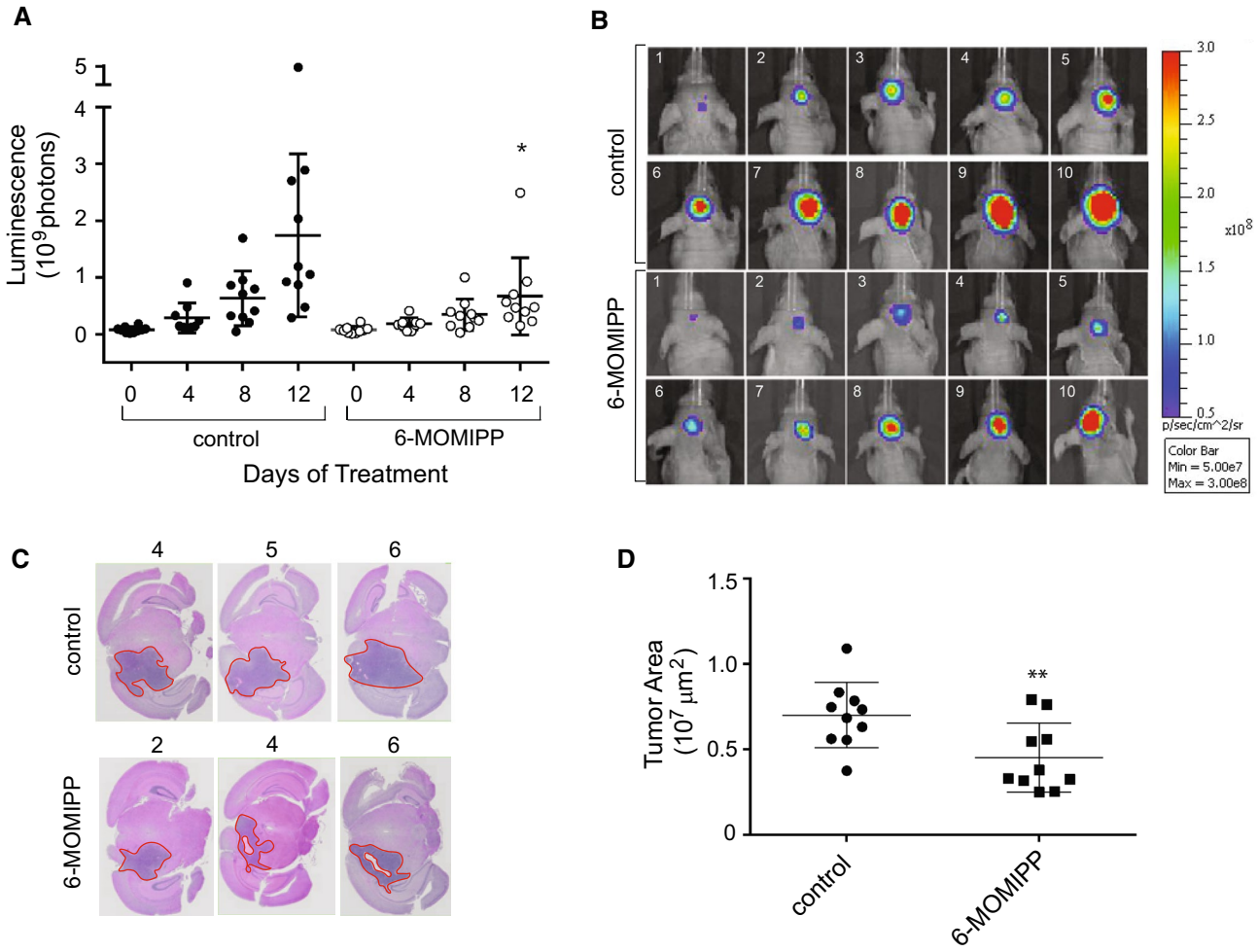

Fig. 6 6-MOMIPP inhibits growth of intracerebral glioblastoma xenografts. Immunocompromised mice received intracranial implants of U251-LUC as described in the "Methods". Treatment with 6-MOMIPP (20 mg/kg, every 12 h) or vehicle was initiated on the 4th day after implantation (designated as day-0). BLI was performed on the mice in the control and 6-MOMIPP groups ($n = 10$) on the indicated days (**a**) and the images from day-12 are depicted in **b**. *The decrease in bioluminescence for the 6-MOMIPP group was significant at $p < 0.01$ on day-12. The brains removed from the control and treated mice were processed for histology and central tumor regions were identified in serial coronal sections. For each tumor, the area was quantified in four separate sections as described in the "Methods", and the mean tumor area was determined. **c** Representative histology images are shown for three mice from each group, with the numbering corresponding to the labels in **b. d** The areas determined for all tumors in the control and treated mice (mean ± SD) are depicted in the graph. **The decrease in the 6-MOMIPP-treated group was significant at $p < 0.01$

the study indicated that the 12-day treatment with 6-MOMIPP did not have adverse effects on glucose, electrolytes, or indicators of liver (alanine transaminase) or kidney (blood urea nitrogen) function. (Online Resource 5). Small but significant decreases were noted in albumin, amylase and phosphorous. The basis for these small changes is unknown.

Discussion

The present studies show that a novel IPP (indolyl-pyridinyl-propenone), 6-MOMIPP, acts as a microtubule-destabilizing agent to induce mitotic arrest and caspase-dependent cell death in glioblastoma and a variety of other cancer cell lines in vitro. The compound also shows significant anti-tumor activity against human glioblastoma xenografts grown subcutaneously in mice. Most importantly, our findings establish that, unlike the majority of MTAs, 6-MOMIPP readily penetrates the BBB and inhibits growth of intracerebral tumors.

In addition to the demonstration of anti-tumor efficacy, the results provide new insights into the mechanism of action of 6-MOMIPP. Using two different approaches, namely SPA and EBI-crosslinking, we show that 6-MOMIPP can compete for occupancy of the colchicine binding site on β-tubulin. Thus, the compound represents a new entry into

the structurally diverse group of MTAs known to interact with this site [57, 58]. While a number of these compounds are chalcone derivatives [23, 24, 59, 60], 6-MOMIPP is structurally unique in terms of having a modified indole ring linked to a pyridinyl moiety via an α,β unsaturated ketone bridge. Unlike closely related IPPs, which trigger vacuolization of endosomal compartments and non-apoptotic cell death via methuosis [25, 26], 6-MOMIPP causes caspase-dependent cell death as a result of disruption of mitotic progression. The DNA histograms, combined with a marked increase in phosphorylation of histone-H3, suggest that cells treated with 6-MOMIPP are arrested in prometaphase prior to caspase activation and cell death. Consistent with this conclusion, treatment with 6-MOMIPP results in marked activation of Cdk1, manifested by phosphorylation of PP1α.

An important consequence of prolonged Cdk1 activation in mitotically arrested cells is phosphorylation of Bcl-2 and Bcl-xL. This is thought to neutralize the anti-apoptotic function of these proteins, contributing to the induction of cell death [45–47]. The importance of Cdk1 activation and Bcl-2/Bcl-xL phosphorylation for cell death induced by 6-MOMIPP is underscored by our finding that a Cdk1 inhibitor, BMS-265246, prevented Bcl-2/Bcl-xL phosphorylation and loss of cell viability. This observation is consistent with previous reports indicating that inhibition of Cdk1 (Cdc2) can block taxol-induced apoptosis in breast cancer cells [61, 62].

Treatment of U251 cells with 6-MOMIPP also resulted in increased phosphorylation and activation of the stress kinase, JNK. Like Cdk1, JNK has been implicated as a mediator of Bcl-2 and Bcl-xL phosphorylation in mitotically arrested cells [63]. Indeed, our studies showed that a JNK inhibitor, SP600125, was able to block Bcl-2/Bcl-xL phosphorylation caused by 6-MOMIPP. Nevertheless, the basis for the ablation of Bcl-2/Bcl-xL phosphorylation by the JNK inhibitor remains controversial, especially in light of the aforementioned studies implicating Cdk1 in this event. One likely possibility is that the effect of SP600125 on Bcl-2/Bcl-xL phosphorylation is indirect, due to the role of JNK in mitotic progression [64, 65]. In other words, cells treated with SP600125 are prevented from completing the transition between G2 and metaphase, where sustained Cdk1 activation occurs during mitotic arrest. Our studies support this concept, since they show that SP600125 blocked cells at a point after completion of DNA replication, but before the phosphorylation of histone-H3 or activation of Cdk1 could be detected.

The ability of 6-MOMIPP to induce mitotic arrest was confirmed in two glioblastoma cell lines, and its ability to inhibit growth and viability was confirmed in multiple human glioblastoma cell lines, as well as in several melanoma and lung cancer lines. However, there were notable differences among the various cell lines in terms of their ability to survive in the presence of 6-MOMIPP. Determining the basis for this differential sensitivity will be an important direction for future study. One factor that could influence the response to mitotic inhibitors is the rate of cell cycling, but this is unlikely to be the sole explanation. For example, among the glioma cell lines, T98G and U251 (most sensitive) and U87MG (least sensitive) have similar doubling times. Another factor that could affect sensitivity to MTAs, particularly those that target the colchicine site, is the expression profile of different β-tubulin isotypes [66, 67]. Finally, cell-type-specific differences in the ability of multidrug resistance transporters to expel 6-MOMIPP may play a role in determining sensitivity. This possibility is supported by our observation that temozolomide-resistant U251 cells and cisplatin-resistant H125 cells were less sensitive to 6-MOMIPP than their non-resistant counterparts. All of these possibilities merit further consideration in future studies.

While 6-MOMIPP was toxic to most of the cancer cell lines at a concentration of 1 μM, the viability of normal fibroblasts and HUVEC was not significantly affected at this concentration. At higher concentration (e.g., 5 μM), the latter cell types were moderately affected, consistent with the fact that they do proliferate at sub-confluent densities. Given the dose-limiting neurotoxicity observed with some MTAs [68], it was particularly interesting to note that 6-MOMIPP had no detectable cytotoxicity in differentiated neuronal cell cultures when applied at 1 or 5 μM. These findings suggest that a therapeutic window exists wherein lower concentrations of 6-MOMIPP may decrease the viability of cancer cells, with minimal effects on normal cells.

Our preliminary PK studies indicated that plasma concentrations well above those required to induce mitotic arrest and cell death in cultured glioblastoma cells (≥ 0.25 μM) could be maintained for at least 8 h following a single ip dose of 6-MOMIPP at 20 mg/kg. Most importantly, there was a striking parallel between plasma and brain concentrations of 6-MOMIPP at all time points, strongly suggesting that the compound freely penetrates the BBB. With one recent exception (ST-11) [69], most MTAs exhibit poor passage across the BBB, limiting their effectiveness for treating primary or secondary brain tumors. Thus, 6-MOMIPP may have potential advantages over the currently available microtubule-destabilizing agents for treatment of brain malignancies. This concept is supported by the results of our studies in mice, which demonstrated that 6-MOMIPP significantly inhibited the progression of both sc and intracerebral glioblastoma xenografts. Given that 6-MOMIPP was well tolerated when administered twice per day for 12 consecutive days, these studies suggest that this new MTA merits further preclinical evaluation as a monotherapy or a combination agent that may synergize with established BBB-penetrant

therapeutic drugs for treatment of glioblastoma and metastatic brain tumors.

Acknowledgements The studies were supported by a grant from the National Institutes of Health (R01 CA115495), the Helen and Harold McMaster Endowment for Biochemistry and Molecular Biology, and the University of Toledo Foundation (James Laur Brain Tumor Research Fund).

Author contributions SD, WAM, JGS and PWE participated in research design. SD, JGS and AS conducted experiments. CJT, JGS and PWE contributed new reagents or analytical tools. SD, JGS and WAM performed data analysis. SD and WAM wrote the manuscript. All authors read and approved the final manuscript.

Compliance with ethical standards

Conflict of interest The compound used in this study, 6-MOMIPP, is included in a patent licensed to Systems Oncology, Inc. As co-inventors, WAM, PWE, and CJT receive a portion of licensing fees and royalties resulting from the licensing agreement. The other authors declare no conflicts of interest.

Ethical approval All animal studies were performed in compliance with United States Public Health Service Policy on Humane Care and Use of Laboratory Animals, under protocols approved by University of Toledo Institutional Animal Care and Use Committee (Reference number 107491).

Human subjects No human subjects were included in these studies.

References

1. Dumontet C, Jordan MA (2010) Microtubule-binding agents: a dynamic field of cancer therapeutics. Nat Rev Drug Discov 9(10):790–803
2. Perez EA (2009) Microtubule inhibitors: differentiating tubulin-inhibiting agents based on mechanisms of action, clinical activity, and resistance. Mol Cancer Ther 8(8):2086–2095
3. Checchi PM, Nettles JH, Zhou J, Snyder JP, Joshi HC (2003) Microtubule-interacting drugs for cancer treatment. Trends Pharmacol Sci 24(7):361–365
4. Stanton RA, Gernert KM, Nettles JH, Aneja R (2011) Drugs that target dynamic microtubules: a new molecular perspective. Med Res Rev 31(3):443–481
5. Vakifahmetoglu H, Olsson M, Zhivotovsky B (2008) Death through a tragedy: mitotic catastrophe. Cell Death Differ 15(7):1153–1162
6. Orth JD, Loewer A, Lahav G, Mitchison TJ (2012) Prolonged mitotic arrest triggers partial activation of apoptosis, resulting in DNA damage and p53 induction. Mol Biol Cell 23(4):567–576
7. Galan-Malo P, Vela L, Gonzalo O, Calvo-Sanjuan R, Gracia-Fleta L, Naval J, Marzo I (2012) Cell fate after mitotic arrest in different tumor cells is determined by the balance between slippage and apoptotic threshold. Toxicol Appl Pharmacol 258(3):384–393
8. Bates D, Eastman A (2017) Microtubule destabilising agents: far more than just antimitotic anticancer drugs. Br J Clin Pharmacol 83(2):255–268
9. Alifieris C, Trafalis DT (2015) Glioblastoma multiforme: pathogenesis and treatment. Pharmacol Ther 152:63–82
10. Anjum K, Shagufta BI, Abbas SQ, Patel S, Khan I, Shah SAA, Akhter N, Hassan SSU (2017) Current status and future therapeutic perspectives of glioblastoma multiforme (GBM) therapy: a review. Biomed Pharmacother 92:681–689
11. Lin X, DeAngelis LM (2015) Treatment of brain metastases. J Clin Oncol 33(30):3475–3484
12. Greig NH, Soncrant TT, Shetty HU, Momma S, Smith QR, Rapoport SI (1990) Brain uptake and anticancer activities of vincristine and vinblastine are restricted by their low cerebrovascular permeability and binding to plasma constituents in rat. Cancer Chemother Pharmacol 26(4):263–268
13. Fellner S, Bauer B, Miller DS, Schaffrik M, Fankhanel M, Spruss T, Bernhardt G, Graeff C, Farber L, Gschaidmeier H, Buschauer A, Fricker G (2002) Transport of paclitaxel (Taxol) across the blood-brain barrier in vitro and in vivo. J Clin Invest 110(9):1309–1318
14. Rice A, Michaelis ML, Georg G, Liu Y, Turunen B, Audus KL (2003) Overcoming the blood-brain barrier to taxane delivery for neurodegenerative diseases and brain tumors. J Mol Neurosci 20(3):339–343
15. Boyle FM, Eller SL, Grossman SA (2004) Penetration of intra-arterially administered vincristine in experimental brain tumor. Neuro Oncol 6(4):300–305
16. Edwards ML, Stemerick DM, Sunkara PS (1990) Chalcones: a new class of antimitotic agents. J Med Chem 33(7):1948–1954
17. Go ML, Wu X, Liu XL (2005) Chalcones: an update on cytotoxic and chemoprotective properties. Curr Med Chem 12(4):481–499
18. Boumendjel A, Boccard J, Carrupt PA, Nicolle E, Blanc M, Geze A, Choisnard L, Wouessidjewe D, Matera EL, Dumontet C (2008) Antimitotic and antiproliferative activities of chalcones: forward structure-activity relationship. J Med Chem 51(7):2307–2310
19. Orlikova B, Tasdemir D, Golais F, Dicato M, Diederich M (2011) Dietary chalcones with chemopreventive and chemotherapeutic potential. Genes Nutr 6(2):125–147
20. Champelovier P, Chauchet X, Hazane-Puch F, Vergnaud S, Garrel C, Laporte F, Boutonnat J, Boumendjel A (2013) Cellular and molecular mechanisms activating the cell death processes by chalcones: critical structural effects. Toxicol In Vitro 27(8):2305–2315
21. Kumar D, Kumar NM, Akamatsu K, Kusaka E, Harada H, Ito T (2010) Synthesis and biological evaluation of indolyl chalcones as antitumor agents. Bioorg Med Chem Lett 20(13):3916–3919
22. Martel-Frachet V, Kadri M, Boumendjel A, Ronot X (2011) Structural requirement of arylindolylpropenones as anti-bladder carcinoma cells agents. Bioorg Med Chem 19(20):6143–6148
23. Boumendjel A, McLeer-Florin A, Champelovier P, Allegro D, Muhammad D, Souard F, Derouazi M, Peyrot V, Toussaint B, Boutonnat J (2009) A novel chalcone derivative which acts as a microtubule depolymerising agent and an inhibitor of P-gp and BCRP in in-vitro and in-vivo glioblastoma models. BMC Cancer 9:242
24. Yan J, Chen J, Zhang S, Hu J, Huang L, Li X (2016) Synthesis, evaluation, and mechanism study of novel indole-chalcone derivatives exerting effective antitumor activity through microtubule destabilization in vitro and in vivo. J Med Chem 59(11):5264–5283
25. Robinson MW, Overmeyer JH, Young AM, Erhardt PW, Maltese WA (2012) Synthesis and evaluation of indole-based chalcones as inducers of methuosis, a novel type of nonapoptotic cell death. J Med Chem 55(5):1940–1956
26. Maltese WA, Overmeyer JH (2014) Methuosis: nonapoptotic cell death associated with vacuolization of macropinosome and endosome compartments. Am J Pathol 184(6):1630–1642
27. Trabbic CJ, Overmeyer JH, Alexander EM, Crissman EJ, Kvale HM, Smith MA, Erhardt PW, Maltese WA (2015) Synthesis and biological evaluation of indolyl-pyridinyl-propenones having either methuosis or microtubule disruption activity. J Med Chem 58(5):2489–2512

28. Trabbic CJ, George SM, Alexander EM, Du S, Offenbacher JM, Crissman EJ, Overmeyer JH, Maltese WA, Erhardt PW (2016) Synthesis and biological evaluation of isomeric methoxy substitutions on anti-cancer indolyl-pyridinyl-propenones: effects on potency and mode of activity. Eur J Med Chem 122:79–91
29. Morrison KC, Hergenrother PJ (2012) Whole cell microtubule analysis by flow cytometry. Anal Biochem 420(1):26–32
30. Laemmli UK (1970) Cleavage of structural proteins during the assembly of the head of bacteriophage T4. Nature 227:680–685
31. Maltese WA, Wilson S, Tan Y, Suomensaari S, Sinha S, Barbour R, McConlogue L (2001) Retention of the Alzheimer's amyloid precursor fragment C99 in the endoplasmic reticulum prevents formation of amyloid beta-peptide. J Biol Chem 276(23):20267–20279
32. Fortin S, Lacroix J, Cote MF, Moreau E, Petitclerc E, Rene C (2010) Quick and simple detection technique to assess the binding of antimicrotubule agents to the colchicine-binding site. Biol Proced Online 12(1):113–117
33. Ozawa T, James CD (2010) Establishing intracranial brain tumor xenografts with subsequent analysis of tumor growth and response to therapy using bioluminescence imaging. J Vis Exp 41:e1986
34. Blagosklonny MV (2007) Mitotic arrest and cell fate: why and how mitotic inhibition of transcription drives mutually exclusive events. Cell Cycle 6(1):70–74
35. Portugal J, Mansilla S, Bataller M (2010) Mechanisms of drug-induced mitotic catastrophe in cancer cells. Curr Pharm Des 16(1):69–78
36. Overmeyer JH, Young AM, Bhanot H, Maltese WA (2011) A chalcone-related small molecule that induces methuosis, a novel form of non-apoptotic cell death, in glioblastoma cells. Mol Cancer 10(1):69
37. O'Reilly KC, Trent S, Bailey SJ, Lane MA (2007) 13-cis-Retinoic acid alters intracellular serotonin, increases 5-HT1A receptor, and serotonin reuptake transporter levels in vitro. Exp Biol Med (Maywood) 232(9):1195–1203
38. Jordan MA, Wilson L (2004) Microtubules as a target for anticancer drugs. Nat RevCancer 4(4):253–265
39. Tahir SK, Kovar P, Rosenberg SH, Ng SC (2000) Rapid colchicine competition-binding scintillation proximity assay using biotin-labeled tubulin. Biotechniques 29(1):156–160
40. Rhind N, Russell P (2012) Signaling pathways that regulate cell division. Cold Spring Harb Perspect Biol 4(10):a005942
41. Chow JP, Poon RY, Ma HT (2011) Inhibitory phosphorylation of cyclin-dependent kinase 1 as a compensatory mechanism for mitosis exit. Mol Cell Biol 31(7):1478–1491
42. Matheson CJ, Backos DS, Reigan P (2016) Targeting WEE1 kinase in cancer. Trends Pharmacol Sci 37(10):872–881
43. Manchado E, Guillamot M, Malumbres M (2012) Killing cells by targeting mitosis. Cell Death Differ 19(3):369–377
44. Ubersax JA, Woodbury EL, Quang PN, Paraz M, Blethrow JD, Shah K, Shokat KM, Morgan DO (2003) Targets of the cyclin-dependent kinase Cdk1. Nature 425(6960):859–864
45. Terrano DT, Upreti M, Chambers TC (2010) Cyclin-dependent kinase 1-mediated Bcl-xL/Bcl-2 phosphorylation acts as a functional link coupling mitotic arrest and apoptosis. Mol Cell Biol 30(3):640–656
46. Yang JS, Hour MJ, Huang WW, Lin KL, Kuo SC, Chung JG (2010) MJ-29 inhibits tubulin polymerization, induces mitotic arrest, and triggers apoptosis via cyclin-dependent kinase 1-mediated Bcl-2 phosphorylation in human leukemia U937 cells. J Pharmacol Exp Ther 334(2):477–488
47. Sakurikar N, Eichhorn JM, Chambers TC (2012) Cyclin-dependent kinase-1 (Cdk1)/cyclin B1 dictates cell fate after mitotic arrest via phosphoregulation of antiapoptotic Bcl-2 proteins. J Biol Chem 287(46):39193–39204
48. Kwon YG, Lee SY, Choi Y, Greengard P, Nairn AC (1997) Cell cycle-dependent phosphorylation of mammalian protein phosphatase 1 by cdc2 kinase. Proc Nat Acad Sci USA 94(6):2168–2173
49. Misra RN, Xiao H, Rawlins DB, Shan W, Kellar KA, Mulheron JG, Sack JS, Tokarski JS, Kimball SD, Webster KR (2003) 1H-Pyrazolo[3,4-b]pyridine inhibitors of cyclin-dependent kinases: highly potent 2,6-difluorophenacyl analogues. Bioorg Med Chem Lett 13(14):2405–2408
50. Prigent C, Dimitrov S (2003) Phosphorylation of serine 10 in histone H3, what for? J Cell Sci 116(18):3677–3685
51. Hu YL, Li S, Shyy JY, Chien S (1999) Sustained JNK activation induces endothelial apoptosis: studies with colchicine and shear stress. Am J Physiol 277(4 pt 2):H1593–H1599
52. Yang Y, Zhu X, Chen Y, Wang X, Chen R (2007) p38 and JNK MAPK, but not ERK1/2 MAPK, play important role in colchicine-induced cortical neurons apoptosis. Eur J Pharmacol 576(1–3):26–33
53. Upreti M, Galitovskaya EN, Chu R, Tackett AJ, Terrano DT, Granell S, Chambers TC (2008) Identification of the major phosphorylation site in Bcl-xL induced by microtubule inhibitors and analysis of its functional significance. J Biol Chem 283(51):35517–35525
54. Bates D, Feris EJ, Danilov AV, Eastman A (2016) Rapid induction of apoptosis in chronic lymphocytic leukemia cells by the microtubule disrupting agent BNC105. Cancer Biol Ther 17(3):291–299
55. Lee SH, Park SW, Pyo CW, Yoo NK, Kim J, Choi SY (2009) Requirement of the JNK-associated Bcl-2 pathway for human lactoferrin-induced apoptosis in the Jurkat leukemia T cell line. Biochimie 91(1):102–108
56. Candolfi M, Curtin JF, Nichols WS, Muhammad AG, King GD, Pluhar GE, McNiel EA, Ohlfest JR, Freese AB, Moore PF, Lerner J, Lowenstein PR, Castro MG (2007) Intracranial glioblastoma models in preclinical neuro-oncology: neuropathological characterization and tumor progression. J Neurooncol 85(2):133–148
57. Lu Y, Chen J, Xiao M, Li W, Miller DD (2012) An overview of tubulin inhibitors that interact with the colchicine binding site. Pharm Res 29(11):2943–2971
58. Greene LM, Meegan MJ, Zisterer DM (2015) Combretastatins: more than just vascular targeting agents? J Pharmacol Exp Ther 355(2):212–227
59. Ducki S, Rennison D, Woo M, Kendall A, Chabert JF, McGown AT, Lawrence NJ (2009) Combretastatin-like chalcones as inhibitors of microtubule polymerization. Part 1: synthesis and biological evaluation of antivascular activity. Bioorg Med Chem 17(22):7698–7710
60. Lindamulage IK, Vu HY, Karthikeyan C, Knockleby J, Lee YF, Trivedi P, Lee H (2017) Novel quinolone chalcones targeting colchicine-binding pocket kill multidrug-resistant cancer cells by inhibiting tubulin activity and MRP1 function. Sci Rep 7(1):10298
61. Yu D, Jing T, Liu B, Yao J, Tan M, McDonnell TJ, Hung MC (1998) Overexpression of ErbB2 blocks Taxol-induced apoptosis by upregulation of p21Cip1, which inhibits p34Cdc2 kinase. Mol Cell 2(5):581–591
62. Shen SC, Huang TS, Jee SH, Kuo ML (1998) Taxol-induced p34cdc2 kinase activation and apoptosis inhibited by 12-O-tetradecanoylphorbol-13-acetate in human breast MCF-7 carcinoma cells. Cell Growth Differ 9(1):23–29
63. Fan M, Goodwin M, Vu T, Brantley-Finley C, Gaarde WA, Chambers TC (2000) Vinblastine-induced phosphorylation of Bcl-2 and Bcl-XL is mediated by JNK and occurs in parallel with inactivation of the Raf-1/MEK/ERK cascade. J Biol Chem 275(39):29980–29985
64. Du L, Lyle CS, Obey TB, Gaarde WA, Muir JA, Bennett BL, Chambers TC (2004) Inhibition of cell proliferation and cell cycle progression by specific inhibition of basal JNK activity: evidence

that mitotic Bcl-2 phosphorylation is JNK-independent. J Biol Chem 279(12):11957–11966
65. Lee K, Song K (2008) Basal c-Jun N-terminal kinases promote mitotic progression through histone H3 phosphorylation. Cell Cycle 7(2):216–221
66. Tseng CY, Mane JY, Winter P, Johnson L, Huzil T, Izbicka E, Luduena RF, Tuszynski JA (2010) Quantitative analysis of the effect of tubulin isotype expression on sensitivity of cancer cell lines to a set of novel colchicine derivatives. Mol Cancer 9:131
67. Parker AL, Teo WS, McCarroll JA, Kavallaris M (2017) An emerging role for tubulin isotypes in modulating cancer biology and chemotherapy resistance. Int J Mol Sci 18(7):1434
68. Carlson K, Ocean AJ (2011) Peripheral neuropathy with microtubule-targeting agents: occurrence and management approach. Clin Breast Cancer 11(2):73–81
69. Cherry AE, Haas BR, Naydenov AV, Fung S, Xu C, Swinney K, Wagenbach M, Freeling J, Canton DA, Coy J, Horne EA, Rickman B, Vicente JJ, Scott JD, Ho RJ, Liggitt D, Wordeman L, Stella N (2016) ST-11: a new brain-penetrant microtubule-destabilizing agent with therapeutic potential for glioblastoma multiforme. Mol Cancer Ther 15(9):2018–2029